



Evolution of Increased Volcanic Activity in Arjuno-Welirang Based on LST Analysis of Landsat 8 Satellite Imagery Using GEE Cloud Computing

Daeng Achmad Suaidi^{1,2}, Sukir Maryanto^{1*}, Didik Rahadi Santoso¹, Agus Naba¹, Muhammad Fathur Rouf Hasan^{1,3}, Siti Zulaikah², Mustaffa Anjang Ahmad⁴, Adnan Zainorabidin⁴

¹Department of Physics, Faculty of Natural Sciences, Brawijaya University, Malang 65145, INDONESIA

²Department of Physics, Faculty of Natural Sciences, Universitas Negeri Malang, Malang 65145, INDONESIA

³Department of Civil Engineering, Politeknik Negeri Jakarta, Depok 16425, INDONESIA

⁴Center of Applied Geomatic and Disaster Prevention, Faculty of Civil Engineering and Built Environmental, Universiti Tun Hussein Onn Malaysia, 86400 Parit Raja, Johor, MALAYSIA

*Corresponding Author

DOI: <https://doi.org/10.30880/ijie.2023.15.07.018>

Received 12 May 2023; Accepted 09 October 2023; Available online 31 December 2023

Abstract: Typically, monitoring the volcanic activity of a volcano is carried out using volcanic seismic methods. However, this method is technically less flexible. Volcano seismic data is not freely available. Access to these data centers must be authorized by the data authority. Therefore, it is necessary to use other methods as an alternative. The alternative method used in this study is remote sensing using the Landsat 8 satellite sensors. Landsat 8 satellite imagery data can be freely accessed and easily downloaded. Landsat 8 image analysis is implemented with Google Earth Engine (GEE). GEE is a remote sensing image analysis programming tool with a cloud computing platform. The GEE programming implementation is open source. With GEE, the evolution of Arjuno-Welirang volcanic activity can be monitored accurately. The use of GEE with a cloud computing platform also makes it easier to process large remote sensing data because the downloaded file's size is unlimited. GEE has successfully conducted an LST analysis on Landsat 8 satellite imagery of the Arjuno-Welirang complex area in the 2016-2021 range. The LST calculation is performed by adding the surface emissivity correction obtained based on the NDVI value. According to the results of the LST calculations that have been obtained, the surface temperature in the Arjuna Welirang Crater area experienced the highest increase in 2018, reaching 33.94 °C, with a larger contour size of thermal distribution image than the others. This increase in thermal based volcanic activity is in accordance with the increase in seismic activity monitored by the VSI (Volcanological Survey of Indonesia).

Keywords: GEE, NDVI, LST, Arjuno-Welirang, Landsat 8, VSI

1. Introduction

After dormancy for 66 years, Arjuno-Welirang's volcanic activity increased in 2018 because a type A volcanic earthquake had occurred caused by the movement of magma towards the upper part of the conduit. A plume of smoke coming from a different side of the crater was clearly visible. The heat source and upflow zone associated with andesite are below the peak of Mt. Welirang [1]. Analyzing convergent geochemical data shows that the existing plumbing system at the Lusi eruption site is connected at depth with the Arjuno-Welirang volcanic complex. Therefore, the increased volcanic activity of Arjuno-Welirang can trigger a large impact on the organic-rich sediments in the subsurface layers of the Lusi sedimentary basin. The migration of hydrothermal fluids from volcanic systems into sedimentary basins triggers metamorphic reactions in organic-rich sediments, which can generate ventilating fracture systems on the surface [2]. So actually, the increase in Arjuno-Welirang seismic activity was giving a hazard warning of geological disasters, which in turn can also cause a volcanic eruption that must be watched out for.

Seismology has proven to be a powerful tool for understanding the problems of volcanism. Seismological techniques are used to help understand the physical conditions and dynamics of the volcanic system to contribute to the initiation of prediction and mitigation of hazardous impacts of volcanic activities [3]. However, there is little information on seismic investigation reports relating to the volcanic activity of the Arjuno-Welirang complex. Most research has investigated the potential for geothermal and subsurface structures. Most of the research in this area investigates the potential of geothermal and subsurface structures [4]. Due to the limitations of these data, in this study, a remote sensing method was tested to monitor the evolution of Arjuno-Welirang volcanic activity, the results of which were verified with VSI's seismic recording data. Currently, petabyte-scale remote sensing data is easily accessible and freely downloaded at several institutions, such as the USGS, NOAA, and NASA [5]-[7]. To facilitate the processing of large-scale geospatial data, currently, many high-performance Digital Image Processing (DIP) software have been developed, such as GeoMesa [8], [9], and GEE [10].

The remote sensing image data used in this study is Landsat 8 satellite imagery. NASA (National Aeronautics and Space Administration) launched Landsat 8 satellite in 2013. Landsat 8 has a collection of high volume data, a systematic global collection, high resolution, and multispectral [11]. Remote sensing using Landsat 8 produces large areas to reach areas that are difficult to reach terrestrially, which can later be used in resource management [12]. The Landsat 8 satellite carries two scientific instrument payloads: The Operational Land Imager (OLI) and the Thermal InfraRed Sensor (TIRS). Global landmass seasonality data is captured by both sensors at spatial resolutions of 30 meters (visible, NIR, SWIR), 100 meters (thermal), and 15 meters (panchromatic). OLI provides two new spectral bands for detecting cirrus clouds and observing the coastal zone. TIRS collects data for two narrow spectral bands in the thermal region previously covered by one broad spectral band in Landsats 4–7 [13]. Some case studies using Landsat 8, such as preliminary analysis of volcanic activity at Paluweh Volcano, Indonesia [14], thermal status monitoring of Aso Volcano in southwest Japan [15], and monitoring of water quality during volcanic eruptions in La Palma, Canary Islands, in 2021 [16].

In this study, the analysis of Landsat 8 satellite imagery uses GEE to determine the surface temperature of the Arjuno Welirang crater area using the LST algorithm. Based on the LST values in the 2016-2021 range, the progress of Arjuno-Welirang volcanic activity can be monitored. GEE is an open source programming tool with a cloud computing platform. GEE utilities provide easy access to high-performance computing resources to provide very large geospatial data processing services without experiencing the challenges of current IT [17]. GEE has been widely used by institutions in developed countries with the largest number of journals on remote sensing, and Landsat satellite imagery is the most frequently used satellite image on this platform [18]. While LST algorithm has been widely used by researchers in various remote sensing journals, e.g., [19]- [22]. The diversity of captured LSTs was investigated in relation to the Normalized Difference Vegetation Index (NDVI) values for each crater state of Arjuno Welirang in the 2016-2021 range. NDVI was developed by Rouse et al. [23]. It is obtained that the surface temperature in Mount Arjuna Welirang Crater had a high thermal temperature in 2018, reaching 33.94 °C. This correlates with the highest increase in VSI seismic activity during the 2017-2021 range as well as in 2018 [4].

2. Background

2.1 Geological Overview of the Arjuno-Welirang Complex

The morphological units in the Mount Arjuno-Welirang complex can be divided into seven geomorphological units, namely the body unit of Mount Anjasmoro, the old body of the Arjuno-Welirang complex, the side eruptions of Mount Bulak and Shoulders, the young body of Mount Arjuno-Welirang, the peak of Mount Arjuno-Welirang, the foot of Mount Arjuno-Welirang, and the foot of Mount Penanggungan [24]. The Arjuno-Welirang geological structures that appear are several structural alignments in the NE-SW and NW-SE directions. Surface geothermal manifestations are controlled by the NW-SE and NNE-SSW fault structures, which are accompanied by the emergence of high-temperature solfataric fumaroles with a high magmatic gas content. So according to these volcanic phenomena, the Arjuno-Welirang geothermal area can be classified as a volcanic geothermal system [25].

Administratively, Arjuno-Welirang is located in four districts in the East Java region, namely Malang, Batu City, Mojokerto, and Pasuruan Regencies. The Arjuno-Welirang geological map is shown in Fig.1 [26]. Arjuno-Welirang

volcano is one of 127 active volcanoes in Indonesia. Arjuno-Welirang is a type A volcano that is classified based on the history of its eruption, which means that the history of the eruption was recorded after 1600 AD. The last eruption occurred in 1952, releasing white volcanic ash accompanied by yellowish-white sulfur mud and spreading to several hundred meters from Plupuh Crater.

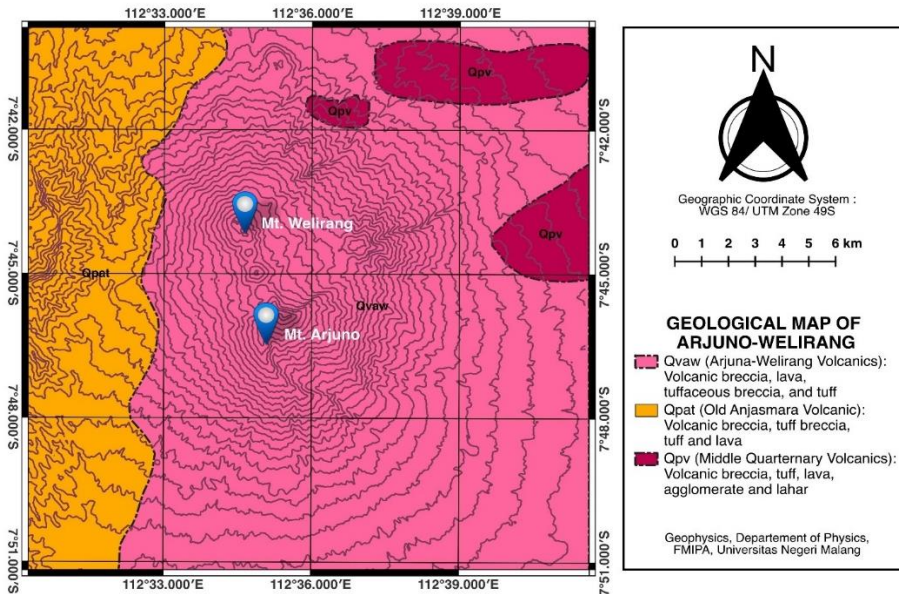


Fig. 1 - Geological map of the Arjuno-Welirang complex [26]

As previously described, the increase in volcanic activity last February 2018 was reported by VSI according to the seismic activity record, as illustrated in Fig. 2. The occurrence of solfatara and fumarole with magmatic gas shows the existence of a subsurface geothermal system that is volcano hosted [1]. The increase in Arjuno-Welirang's volcanic activity in February 2018, as previously explained, was the highest increase in volcanic activity since the last eruption occurred 71 years ago. VSI has reported this increase in activity based on recorded seismic equipment installed, as illustrated in Fig. 2. Solfatara and fumaroles with magmatic gas were visually observed when this increased activity occurred. It indicates the existence of a subsurface geothermal system associated with a volcanic system [1].

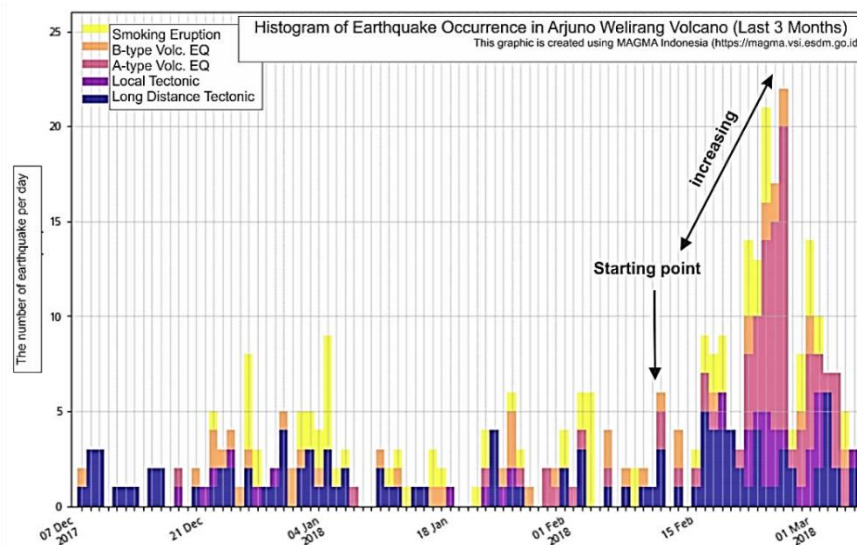


Fig. 2 - Graph of increased volcanic activity in Arjuno-Welirang from December 2017 to March 2018. Recorded by VSI [4]

2.2 Google Earth Engine Code Editor

The Google Earth Engine (GEE) Code Editor at code.earthengine.google.com (illustrated in Fig. 3) is a web-based IDE software for the JavaScript API of the Earth Engine. The Code Editor feature is designed to handle complex

geospatial workflow development tasks quickly and easily. The Code Editor consists of the following elements: JavaScript Code Editor, API Reference Documentation (Documents Tab), Console Output (Console Tab), Git-Based Script Manager (Scripts Tab), Task Manager (Tasks Tab), Interactive Map Queries (Inspector Tab), Geometry Drawing Tool, Search Archived Data (Saved Scripts), Map View [27]. This platform was founded in late 2010 and is a web portal that provides global satellite imagery, cloud-based computing, and access to software and algorithms to process large amounts of data easily [18]. GEE provides cloud computing facilities that can store and process big terrestrial data up to the Petabyte scale. In addition, GEE is open source and can be used by anyone without needing high processing capacity computer equipment. The desired data can be generated by compiling a programming script in the Javascript language.

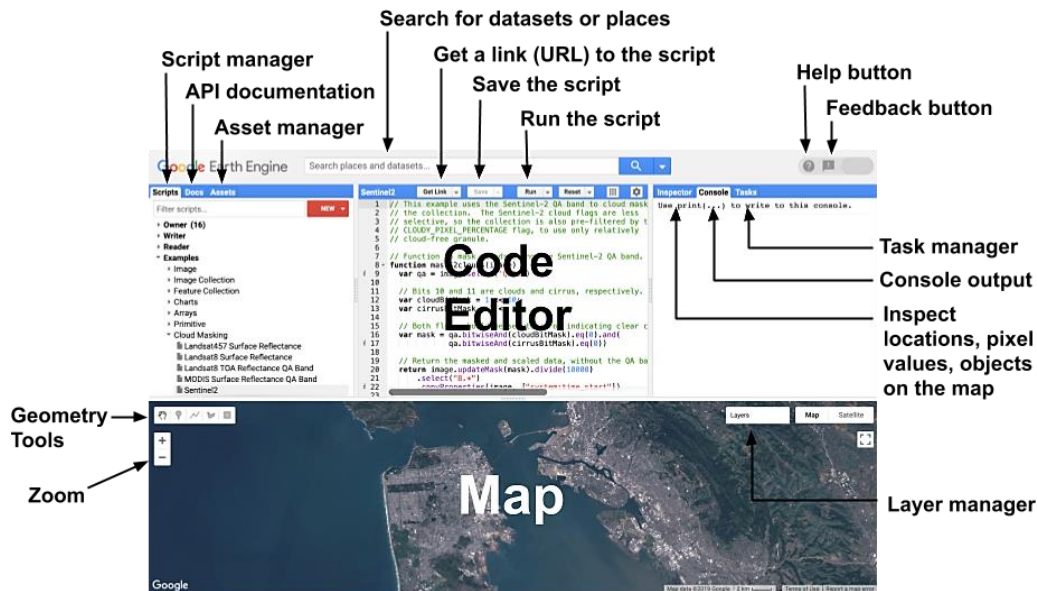


Fig. 3 - Diagram of components of the GEE at code.earthengine.google.com [27]

2.3 Landsat 8

On 11 February 2013, Landsat 8 was launched using an Atlas-V rocket from Vandenberg Air Force Base, California. This satellite carries two main instruments: The Operational Land Imager (OLI) and the Thermal Infrared Sensor (TIRS). OLI was designed and manufactured by Ball Aerospace & Technologies Corporation, while TIRS was by NASA's Goddard Space Flight Center. OLI collects data in the visible, near-infrared, and short-infrared (VNIR, NIR, and SWIR) parts of the spectrum, while TIRS detects ground surface temperatures in two thermal bands by applying quantum physics. The spatial resolution of Landsat 8 imagery is 15 meter panchromatic and 30 meter multispectral over a 185 km (115 mi) swath [28], [29]. There are 11 bands on both sensors. Bands 1 to 9 are on the OLI sensor, while bands 10 and 11 are on TIRS. The 11 bands above can be combined to produce new images in different colors and for different applications. Table 1 presents the characteristics of the 11 bands.

Table 1 - The bands' characteristics on the Landsat 8 [28], [29]

Band	Spectrum	Sensor	Spectral range (μm)	Spatial Resolution (m)
1.	Coastal Aerosol	OLI	0.43-0.45	30
2.	Blue	OLI	0.45-0.51	30
3.	Green	OLI	0.53-0.59	30
4.	Red	OLI	0.64-0.67	30
5.	Near Infrared	OLI	0.85-0.88	30
6.	SWIR1	OLI	1.57-1.65	30
7.	SWIR2	OLI	2.11-2.29	30
8.	Panchromatic	OLI	0.50-0.60	15
9.	Cirrus	OLI	1.36-1.38	30
10.	TIRS1	TIRS	10.60-11.19	100
11.	TIRS2	TIRS	11.50-12.51	100

2.4 LST Algorithms

LST (Land Surface Temperature) is the outermost temperature of the object's surface. This temperature can be observed using satellite images that have thermal sensors such as Landsat 5 and Landsat 8 [25]. The soil surface temperature can be calculated by adding the surface emissivity correction obtained based on the NDVI (Normalized Difference Vegetation Index) value. NDVI is determined based on the near infrared channel's reflectance value and the red channel's reflectance value. The LST calculation is formulated by Eq. (1) [30]. LST calculations were carried out based on Top of Atmosphere (ToA) radiation and BT (Brightness Temperature) satellite images based on NDVI values to determine emissivity values on the earth's surface.

$$LST = \frac{BT}{1 + \left(\lambda \frac{BT}{\rho} \ln(\varepsilon) \right)} - 273 \quad (1)$$

where BT is brightness temperature (K), λ is the wavelength of band 10 or 11 (μm), ε is the spectral surface emissivity, and ρ is $(h \times c / \sigma) = 1.438 \times 10^{-2}$ mK in which, σ is the Boltzmann constant = 1.38×10^{-23} JK⁻¹, h is Plank constant = 6.626×10^{-34} , and c is the velocity of light = 3×10^8 m/s. Finally, LST is Land Surface Temperature ($^{\circ}C$). To calculate the emissivity, ε can use Eq. (2) [21].

$$\varepsilon = 0.986 + 0.004P_v \quad (2)$$

where P_v value represents proportional vegetation formulated by Eq. (3) [31].

$$P_v = \frac{(NDVI - NDVI_s)^2}{(NDVI_v - NDVI_s)} \quad (3)$$

where $NDVI_s$ and $NDVI_v$ represent soil and vegetation NDVI values, respectively.

2.5 Normalized Difference Vegetation Indeks (NDVI)

NDVI is a ratio that expresses the density of vegetation in an area. The NDVI value is calculated from the input reflectance values of the red and near infrared bands using Eq. (4). This vegetation index works by utilizing the difference in spectral energy reflected by the vegetation canopy at the wavelengths of the red and near infrared electromagnetic spectrum [31].

$$NDVI = \frac{\rho_{nir} - \rho_{red}}{\rho_{nir} + \rho_{red}} \quad (4)$$

where ρ_{nir} = reflectance value of the near infrared channel, ρ_{red} = reflectance value of the red channel. For Landsat 8 NDVI values use bands 4 and 5.

3. Methods

The method used in this study is integrating cloud computing-based remote sensing techniques using Google Earth Engine (GEE). The location of this research is the area of the Arjuna-Welirang Volcano Complex which is located in three regencies, namely Malang, Mojokerto, Pasuruan, and Batu City, with coordinates $112^{\circ} 31' 0.57'' - 112^{\circ} 37' 50.6''$ East Longitude and $7^{\circ} 39' 39.2'' - 7^{\circ} 48' 48.1''$ South Latitude. Fig. 4 shows the research location in Map View of GEE, which is loaded by the statement source code in the JavaScript Code Editor element, namely `ee.ImageCollection('LANDSAT/LC08/C01/T1_RT_TOA')`. The inscription `LANDSAT/LC08/C01/T1_RT_TOA` is a Landsat 8 satellite image data file of the Arjuna-Welirang Volcano. The image data is selected from 1 January 2016 to 31 December 2021 using the following source code: `filterDate('2016-01-01', '2021-12-31')`. And to define the research area around the Arjuno-Welirang crater, the following source code is used: `ee.Geometry.Polygon({coords: [[112.5698000, -7.72500000], [112.5850000, -7.72500000], [112.5850000, -7.74000000], [112.5698000, -7.74000000]]})`.

These satellite images are processed to obtain outputs in the form of distribution maps of surface temperature anomalies or LSTs in the Arjuno-Welirang crater area, where changes in the LST distribution from one image to another show changes in volcanic activity in the Arjuno-Welirang crater area during the 2016-2021 timeframe. LST calculation is carried out based on ToA radiation, and the brightness temperature of the satellite image is based on the NDVI value to determine the emissivity value on the earth's surface [7]. Remote sensing data processing in this study aims to determine land cover and the distribution of *LST* in the study area. With this goal, data processing is divided into two processes, namely, the process of obtaining the value of soil emissivity and temperature brightness. Remote sensing data processing is done using the GEE Cloud Computing tool. The flow of data processing can be seen in Fig. 5.

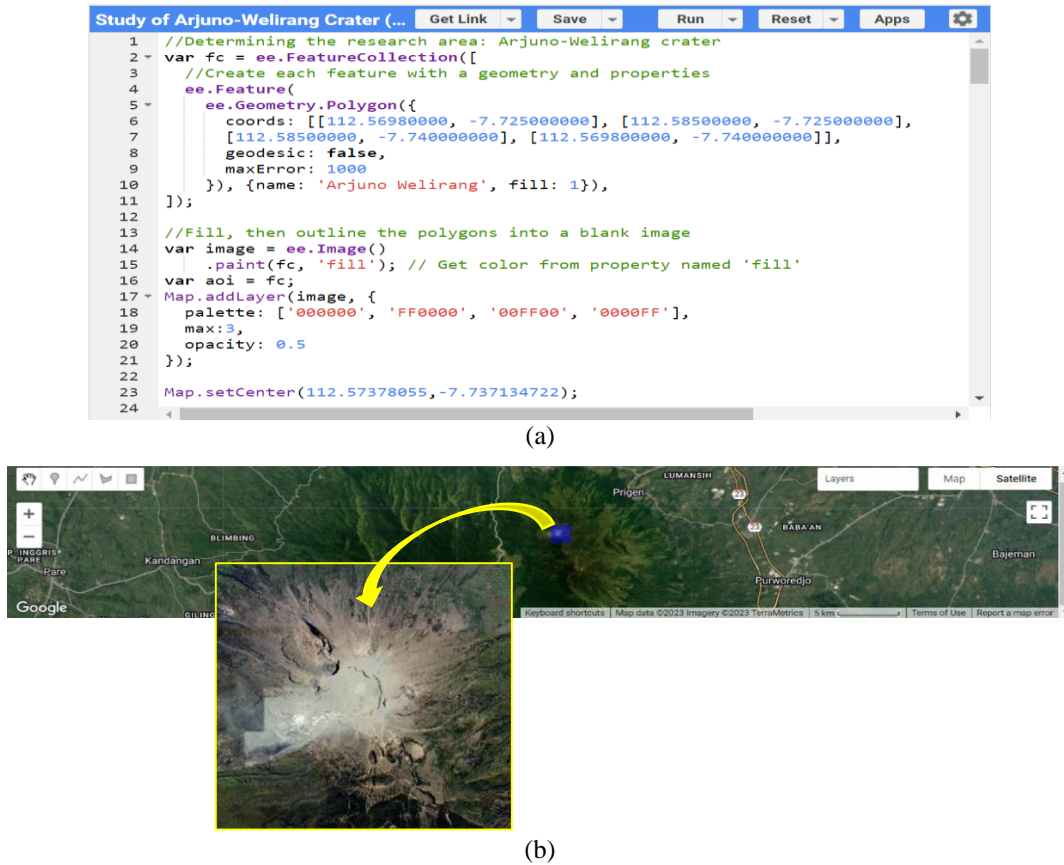


Fig. 4 - The research location in Map View of GEE (a) source code for handling the Arjuno Welirang crater area according to the latitude and longitude data input, and; (b) image display of the Arjuno Welirang crater

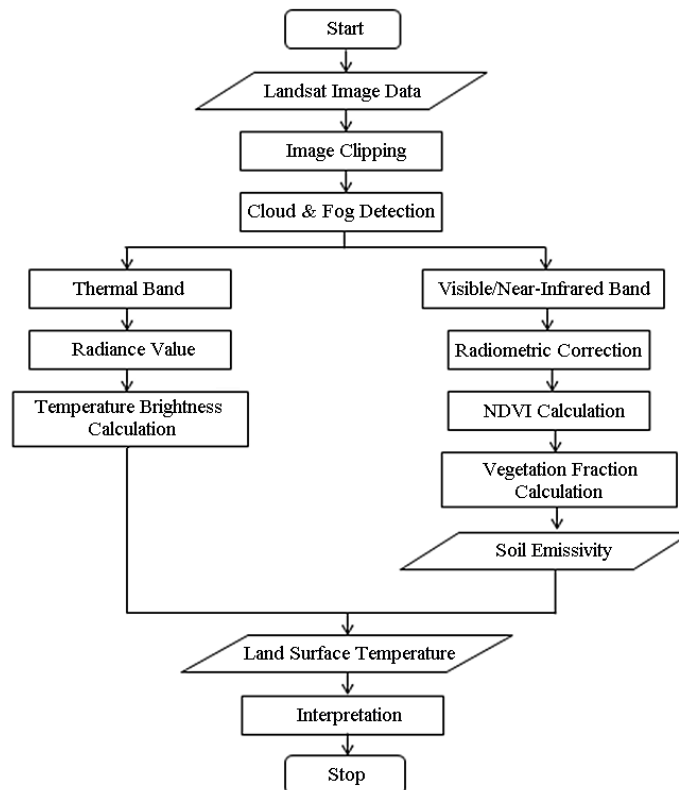


Fig. 5 - LST imaging flowchart of Arjuno-Welirang Crater area with GEE cloud computing

4. Results and Discussion

The data used for LST mapping are as follows: band 4 or red band with a wavelength of 0.64 -0.67 μm, band 5 or near infrared band with a wavelength of 0.85 -0.88 μm, and band 10 or Thermal Infrared band with a wavelength of 10.6 -11.19 μm. Bands 4 and 5 are used to determine the NDVI value using the following source code: `addNDVI=function(image){return image.addBands(image.normalizedDifference(['B5', 'B4']).rename('NDVI'))}`, while band 10 is used to determine the LST value using the following source code: `celsius=image.expression('(B10/(1+(10.8*B10/14388) *log((0.004*((ndvi-0.2)/0.3)+ 0.986)))) - 273.15', {'ndvi':image.select('NDVI'),'B10': image.select('B10')})`. The NDVI value is obtained from the processing carried out on the reflectance values of the near infrared and red channels on the OLI (Operational Land Imager) sensor. Finally, LST values in the Arjuno-Welirang Crater area were obtained from thermal band image processing on the TIRS (Thermal Infrared Sensor). The LST value is obtained using an algorithm by estimating the emissivity and brightness temperature sensors. Temperature brightness is electromagnetic radiation from the Earth's atmosphere.

According to the results of processing and analysis of Landsat 8 satellite imagery from 2016 to 2021 above, the LST values of the Arjuno-Welirang crater area are obtained as follows, the Year 2016: 31.21 °C, the Year 2017: 31.55 °C, the Year 2018: 33.94 °C, the Year 2019: 32.71 °C, 2020: 29.87 °C, 2021: 30.22 °C, which is displayed on the GEE Inspector tab as shown in Fig. 6. More clearly, the average LST values for each year are presented in Table 2. Table 2 shows an illustration of the correlation between changes in the average LST values and changes in years in the 2016-2021 range so that graphs of thermal activity can be plotted in the period 2016 to 2021, as shown in Fig. 7.

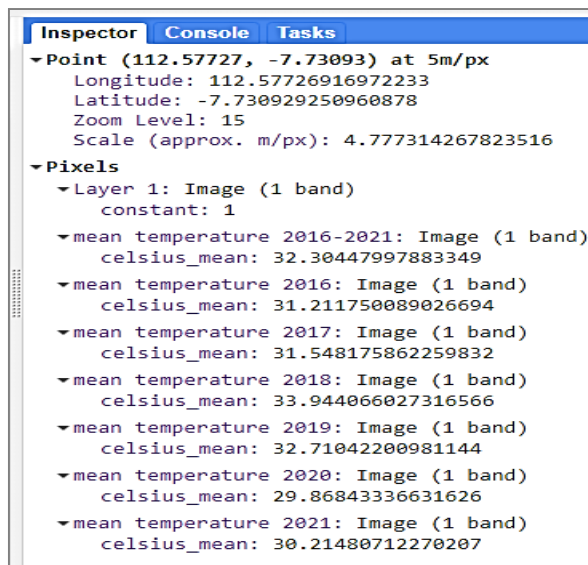


Fig. 6 - LST values generated from the running GEE tool program displayed in text data format on the Inspector Tab

Table 2 - LST values of Arjuno-Welirang crater

Years	LST (°C)
2016	31.21175
2017	31.54818
2018	33.94407
2019	32.71042
2020	29.86843
2021	30.21481

The graph is drawn with a bar chart as well as the VSI seismic activity graph in Fig. 2. This is to make it easier to carry out a comparative analysis which is intended to get a correlation between increased seismic activity and thermal activity, which basically correlates with an increase in Arjuno-Welirang volcanic activity. The graph in Fig. 2 displays an increase in volcanic activity identified based on increased seismic activity. In contrast, Fig. 7 displays increased volcanic activity identified based on increased thermal activity. So, Fig. 2 and Fig. 7 show the same pattern of increasing volcanic activity. The graph in Fig. 2 shows the highest increase in volcanic activity in 2018 as well as the graph in Fig. 7. The Arjuno-Welirang Crater area had high thermal activity in 2018, reaching a temperature of 33.94 °C, indicating that the mountain is experiencing an increase in volcanic activity.

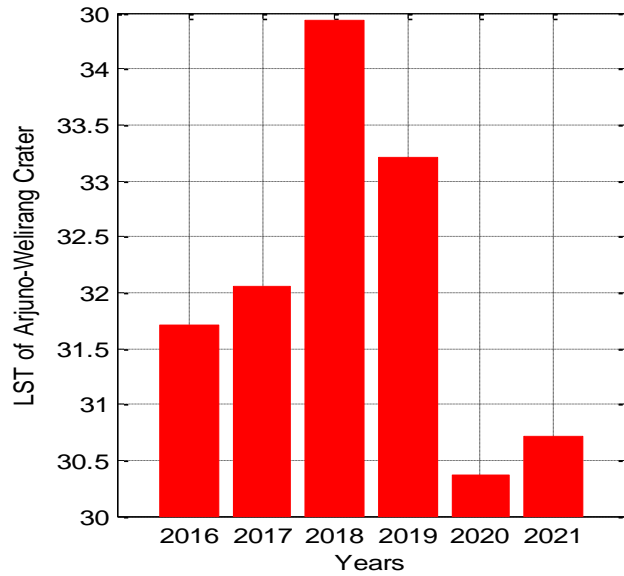


Fig. 7 - LST values overall years are plotted in graph

LST imagery provides an evolutionary map of surface temperature anomalies in the Arjuno-Welirang crater area, as illustrated in Fig. 8. Changes in the distribution of LST values from one image to another show changes in thermal activity that correlate with changes in volcanic activity in the Arjuno-Welirang crater area during 2016-2021. In this image, changes in volcanic activity are expressed by changing the image's color and changing the size of the map contours. The map legend displays image color gradations. The dark blue color represents the lowest temperature, and the dark red color represents the highest temperature. The largest contour size in dark red in the Arjuno-Welirang crater area is shown by the 2018 LST imagery, which means that the highest increase in volcanic activity occurred in 2018.

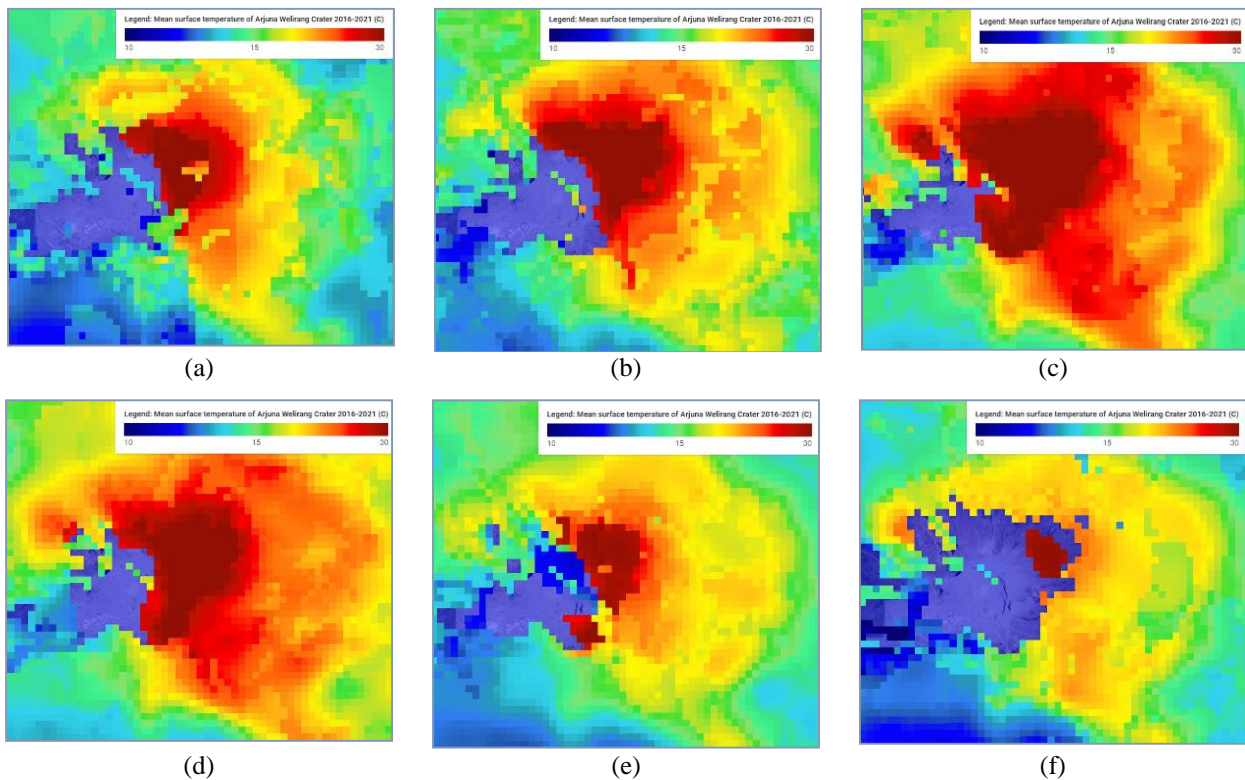


Fig. 8 - Evolution of average LST imaging in the area of the Arujuno Welirang crater in 2016–2021 (a) 2016 - 31.21 °C; (b) 2017 - 31.55 °C; (c) 2018 - 33.94 °C; (d) 2019 - 32.71 °C; (e) 2020 - 29.87 °C, and; (f) 2021 - 30.22 °C

The analysis results of the LST graphs and images above show that an increase in volcanic activity causes an increase in thermal activity which is identified from the LST value and its distribution. The LST graph explicitly presents the

increase in LST value, while the increase in the size of the LST spreading contour is visually shown by LST imagery. The highest temperature with the largest contour size of thermal distribution in the Arjuno-Welirang crater area is shown in 2018. Both the graphical and image analysis results correlate with an increase in seismic activity monitored by VSI, as shown in Fig. 2. VSI installed a seismic station to monitor Arjuno-Welirang activity since 1995. VSI records show increased volcanic activity in Arjuno-Welirang starting in early February 2018 [4].



Fig. 9 - Average LST time series chart in the Arujuno Welirang crater area in 2016–2021

The daily data is shown in Fig. 9. It can be seen that an increase in volcanic activity occurred in 2018. This is in accordance with the development of the LST image changes in Fig. 8. However, the visual appearance of the curve is not suitable for monitoring daily volcanic activity because the Landsat 8 sensor records data every 16 days. The Landsat 8 sensors overpass every Earth location every 16 days (i.e., no more than twice per month), but the observed number of acquisitions in any month can be greater than two because of the across-track scene overlap [32]. Even so, the evolution of annual volcanic activity can be shown well based on changes in LST imagery as explained previously based on imaging visualization in Fig. 8. For subsequent studies, it is necessary to design and build a GEE computing based on combined sensor data Landsat 8 and Landsat 7 to better visualize the development curve of Arjuno Welirang volcanic activity. Combined the Landsat 8 and 7 sensors provide the ability to acquire a WRS-2 (The Second Worldwide Reference System) track every 8 days at the Equator and more frequent coverage at higher latitudes due to the polar convergence of Landsat orbits [32].

5. Conclusion

The evolution of Arjuno-Welirang volcanic activity in the 2016-2021 timeframe can be monitored by surface temperature imaging based on analysis of Landsat 8 imagery using LST and NDVI algorithms implemented with Google Earth Engine cloud computing programming. From 2016 to 2021, the Arjuno-Welirang Crater area had the highest thermal activity in 2018, reaching a temperature of 33.94 °C with a larger contour size of thermal distribution than the others, which indicates that the mountain is experiencing an increase in volcanic activity. This increase in thermal activity correlates with an increase in seismic activity reported on the VSI seismic record. The method used in this study is unsuitable for displaying daily volcanic activity because the Landsat 8 sensor records data every 16 days; even so, the evolution of annual volcanic activity can be shown well based on changes in LST imagery. For further research, it is necessary to design and implement the GEE programming using Landsat 8 and 7 combined data. With this combined data, it is expected that the quality of information on Arjuno Welirang volcanic activity will increase two times better, with data acquisition every 8 days.

Acknowledgement

This work was supported by Brawijaya Volcanology and Geothermal Research Center, Center for Energy and Natural Resources Studies Brawijaya University East Java Indonesia, Department of Physics Faculty of Natural Sciences Brawijaya University East Java Indonesia, Department of Physics Faculty of Natural Sciences State University of Malang, East Java Indonesia.

References

- [1] Geological Agency of Indonesia (2011). Volcanoes Data in Indonesia. Geological Agency of Indonesia, pp. 400-411.
- [2] Inguaggiato S., Mazzini A. Vita F. & Sciarra A. (2018). The Arjuno-Welirang volcanic complex and the connected Lusi system: Geochemical evidences. *Marine and Petroleum Geology*, 90, 67-76.
- [3] Kawakatsu H. & Yamamoto M. (2015). Volcano seismology. *Treatise on Geophysics*, 4, 389-419.
- [4] Maryanto S. (2018). Microseismicity recorded at Cangar, Arjuno-Welirang volcano-hosted geothermal complex, Batu City, East Java, Indonesia. *AIP Conference Proceedings*, (1), 030017.

- [5] Loveland T. R. & Dwyer J. L. (2012). Landsat: Building a strong future. *Remote Sensing of Environment*, 122, 22-29.
- [6] Nemani R., Votava P., Michaelis A., Melton F. & Milesi C. (2011). Collaborative Supercomputing for Global Change Science. *Eos, Transactions American Geophysical Union*, 92, 109-110.
- [7] Woodcock C. E., Allen R., Anderson M., Belward A., Bindschadler R., Cohen W., Gao F., Goward S. N., Helder D., Helmer E., Nemani R., Oreopoulos L., Schott J., Thenkabail P. S., Vermote E. F., Vogelmann J., Wulder M. A. & Wynne R. (2008). Free access to Landsat imagery. *Science*, 320, 1011.
- [8] Hughes J. N., Annex A., Eichelberger C. N., Fox A., Hulbert A. & Ronquest M. (2015). GeoMesa: A distributed architecture for spatio-temporal fusion. *Geospatial Informatics, Fusion, and Motion Video Analytics V*, 9473, 128-140.
- [9] Yu J., Wu J. & Sarwat M. (2015). GeoSpark: A cluster computing framework for processing large-scale spatial data. *GIS: Proceedings of the ACM International Symposium on Advances in Geographic Information Systems*, 70, 1-4.
- [10] Google's Cloud Infrastructure (2023). Earth Engine Signup. Google Earth Engine. <https://signup.earthengine.google.com/#/>
- [11] Zanter K. (2019). LANDSAT 8 (L8) Data Users Handbook (LSDS-1574 Version 5.0). United States Geological Survey.
- [12] Roy D. P., Wulder M. A., Loveland T. R., Allen R. G., Anderson M. C., Helder D., Irons J. R., Johnson D. M., Kennedy R., Scambos T. A., Schaaf C. B., Schott J. R., Sheng Y., Vermote E. F., Belward A. S., Bindschadler R., Cohen W. B., Gao F. & Zhu Z. (2014). Landsat-8: Science and product vision for terrestrial global change research. *Remote Sensing of Environment*, 145, 154-172.
- [13] National Aeronautics and Space Administration (2023). Landsat 8 Mission Details. [https://landsat.gsfc.nasa.gov/Satellites/Landsat 8/Landsat-8-Mission-Details/](https://landsat.gsfc.nasa.gov/Satellites/Landsat%208/Landsat-8-Mission-Details/)
- [14] Blackett M. (2014). Early analysis of Landsat-8 thermal infrared sensor imagery of volcanic activity. *Remote Sensing*, 6(3), 2282-2295.
- [15] Mia M. B., Fujimitsu Y. & Nishijima J. (2017). Thermal Activity monitoring of an active volcano using Landsat 8/OLI-TIRS sensor images: A case study at the aso volcanic area in Southwest Japan. *Geosciences*, 7(4), 118.
- [16] Caballero I., Román A., Tovar-Sánchez A. & Navarro G. (2022). Water quality monitoring with Sentinel-2 and Landsat-8 satellites during the 2021 volcanic eruption in La Palma (Canary Islands). *Science of The Total Environment*, 822, 153433.
- [17] Gorelick N., Hancher M., Dixon M., Ilyushchenko S., Thau D. & Moore R. (2017). Google Earth Engine: Planetary-scale geospatial analysis for everyone. *Remote Sensing of Environment*, 202, 18-27.
- [18] Kumar L. & Mutanga O. (2018). Google Earth engine applications since inception: Usage, trends, and potential. *Remote Sensing*, 10, 1509.
- [19] Narayana Reddy S. & Manikiam B. (2017). Land surface temperature retrieval from LANDSAT data using emissivity estimation. *International Journal of Applied Engineering Research*, 12, 9679-9687.
- [20] Rehman Z., Kazmi S. J. H., Khanum F. & Samoon Z. A. (2015). Analysis of land surface temperature and NDVI using geo-spatial technique: A case study of Keti Bunder, Sindh, Pakistan. *Journal of Basic and Applied Sciences*, 11, 514-527.
- [21] Sobrino J. A., Jiménez-Muñoz J. C. & Paolini L. (2004). Land surface temperature retrieval from LANDSAT TM5. *Remote Sensing of Environment*, 90(4), 434-440.
- [22] Sukojo B. & Anjasmara I. M. (2016). The analysis of surface temperature anomalies at Arjuno-Welirang geothermal prospects using multitemporal thermal infrared (TIR) remote sensing data. *The 2nd ISST 2016 – International Seminar on Science and Technology*, pp. 399-400.
- [23] Rouse J. W., Jr., Haas R. H., Deering D. W., Schell J. A. & Harlan J. C. (1974). Monitoring the Vernal Advancement and Retrogradation (Green Wave Effect) of Natural Vegetation. Texas A&M University.
- [24] Hadi M. N. & Kusnadi D. (2010). Penyelidikan terpadu geologi dan geokimia daerah panas bumi Arjuno-Welirang, Jawa Timur. *Prosiding Hasil Kegiatan Pusat Sumber Daya Geologi*, pp. 205-416.
- [25] Daud Y., Nuqramadha W. A., Fahmi F., Sesesega R. S., Fitrianita, Pratama S. A. & Munandar A. (2019). Resistivity characterization of the Arjuno-Welirang volcanic geothermal system (Indonesia) through 3-D magnetotelluric inverse modeling. *Journal of Asian Earth Sciences*, 174, 352-363.
- [26] Santosa S. & Suwarti T. (1992). Peta Geologi Lembar Malang, Jawa (Geological Map of The Malang Quadrangle, Jawa). Geological Research and Development Centre.
- [27] Google Earth Engine (2023). Earth Engine Code Editor. <https://developers.google.com/earth-engine/guides/playground>.
- [28] USGS (2023). Landsat 8. <https://www.usgs.gov/landsat-missions/landsat-8>
- [29] Li S. & Jiang G. M. (2018). Land surface temperature retrieval from Landsat-8 data with the generalized split-window algorithm. *IEEE Access*, 6, 18149-18162.
- [30] Stathopoulou M. & Cartalis C. (2007). Daytime urban heat islands from Landsat ETM+ and Corine land cover data: An application to major cities in Greece. *Solar Energy*, 81(3), 358-368.

- [31] Carlson T. N. & Ripley D. A. (1997). On the relation between NDVI, fractional vegetation cover, and leaf area index. *Remote Sensing of Environment*, 62(3), 241-252.
- [32] Kovalsky V. & Roy D. P. (2013). The global availability of Landsat 5 TM and Landsat 7 ETM+ land surface observations and implications for global 30 m Landsat data product generation. *Remote Sensing of Environment*, 130, 280-293.